4 cERL

4-1 Status of the cERL Project

In order to demonstrate key technologies for the ERL light-source project, we are constructing the Compact ERL (cERL) [1, 2] at KEK. The cERL will be commissioned at the end of FY2012. During 2011, we worked on designing an initial plan for the cERL at a beam energy of 35 MeV. Figure 1 shows the current plan of the cERL for commissioning. It will comprise a 5-MeV injector including a 500-kV DC photocathode gun and three two-cell superconducting (SC) cavities, a main SC linac having a single cryomodule, single return loop, and supporting facilities. The principal parameters of the cERL are shown in Table 1.

In the following sections, we report the design and construction status of the cERL. We then report the status of R&D efforts on a high-brightness gun, SC cavities, and helium refrigerator system.

REFERENCES

[1] R. Hajima, N. Nakamura, S. Sakanaka, and Y. Kobayashi (ed.), *KEK Report* 2007- 7 (2008)/*JAEA-Research* (2008) 032 .
[2] See, for example, S. Sakanaka, H. Kawata, Y. Kobayashi, N. Nakamura, R. Hajima, *Proc. LINAC'10* (2010) 398.

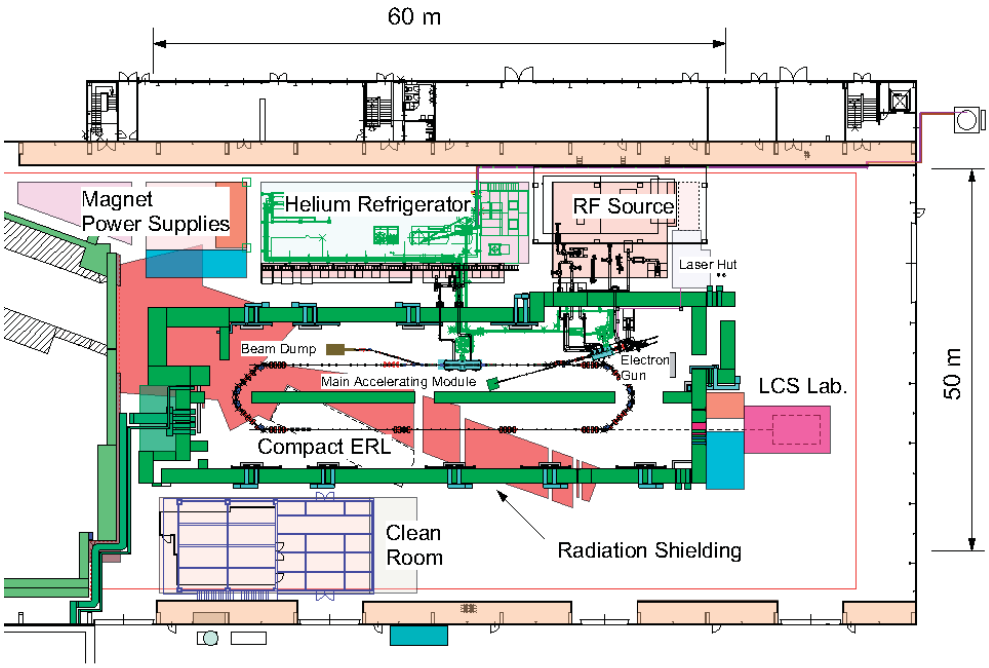

Figure 1
Current plan of the Compact ERL for commissioning.

Table 1 Parameters of the Compact ERL.

Parameter	Initial goal	Final goal
Beam energy at recirculation	35 MeV (single loop)	125 MeV (single loop) 245 MeV (double loops)
Injection energy	5 MeV	5 MeV
Average beam current	10 mA	100 mA
RF frequency	1.3 GHz	1.3 GHz
Accelerating gradient of main SC cavities	15 MV/m	15 MV/m
Bunch repetition frequency	1.3 GHz	1.3 GHz
Normalized emittance	1 mm·mrad	1 mm·mrad (77 pC/bunch) 0.1 mm·mrad (7.7 pC/bunch)

4-2 Design of cERL

4-2-1 Design of Injector

Since the brilliance of electron beams in the ERLs is primarily determined by the injector, the design and performance of the injector is critical. Figure 2 shows our injector design for the cERL. It consists of a high-brightness photocathode DC gun, two solenoid magnets, a bunching cavity, and three 2-cell SC cavities. Electron beams are generated from the cathode surface of the electron gun, and accelerated to 500 keV. The beams are then accelerated through the injector cavities up to a beam energy of 5 MeV (or 10 MeV in case of the ERL light source). After the injector cavities, the beams are matched using five quadrupole magnets, and then injected to the main linac through a merger section; the merger comprises three dipole magnets and two quadrupoles. To preserve small beam emittance, it is important to manage emittance growth due to the combined effect of space charge and dispersion function in the merger. For this purpose, the strengths of the five quadrupoles before the merger are optimized.

Because the beam energy is low, the motions of the beams are largely influenced by self-forces due to space charge, as well as by focusing forces due to RF fields. The beam dynamics in the injector are therefore very complicated. In order to produce high-brilliance beams from the injector, we optimized the beamline parameters of the injector by applying a multi-objective method based on a genetic algorithm. In this method, the beamline from the gun to an exit of the main SC cavities is modeled using a particle tracking code, GPT, which can handle three-dimensional space-charge effect. During the optimization, we carried out two important tasks: 1) minimization of the emittance, and 2) matching of beam optics to that of the return loop. To match the beam optics, we adjusted the Twiss parameters at the exit of the main-linac cavities so that reasonable beam optics could be designed throughout the return loop. We repeated this process until we could obtain good designs for both the injector and the return loop.

Under the first commissioning of the cERL, the bunch charge and the beam energy from the injector will be limited to 7.7 pC/bunch and 5 MeV, respectively. We are currently optimizing the beamline parameters under this condition by looking at the beam parameters at an exit (called the “matching point” hereafter) of the first main-linac cavity where the beam energy is 35 MeV. Typical results of optimization are shown in Fig. 3 and Table 2. In this optimization, we set our target Twiss parameters at the matching point to be: $-2.0 < \alpha_x < 0$, $0 < \alpha_y < 2.0$, $0.5\ \mathrm{m} < \beta_x < 15\ \mathrm{m}$, and $0.5\ \mathrm{m} < \beta_y < 15\ \mathrm{m}$, which are required by the optics design of the return loop. It should be noted that the normalized emittance shown in Fig. 3 (1.1 mm·mrad at the matching point) is not small enough. At present, we have experienced some conflict between the optimization of injector and the restriction of Twiss parameters at the matching point, and so we are trying to optimize the design further.

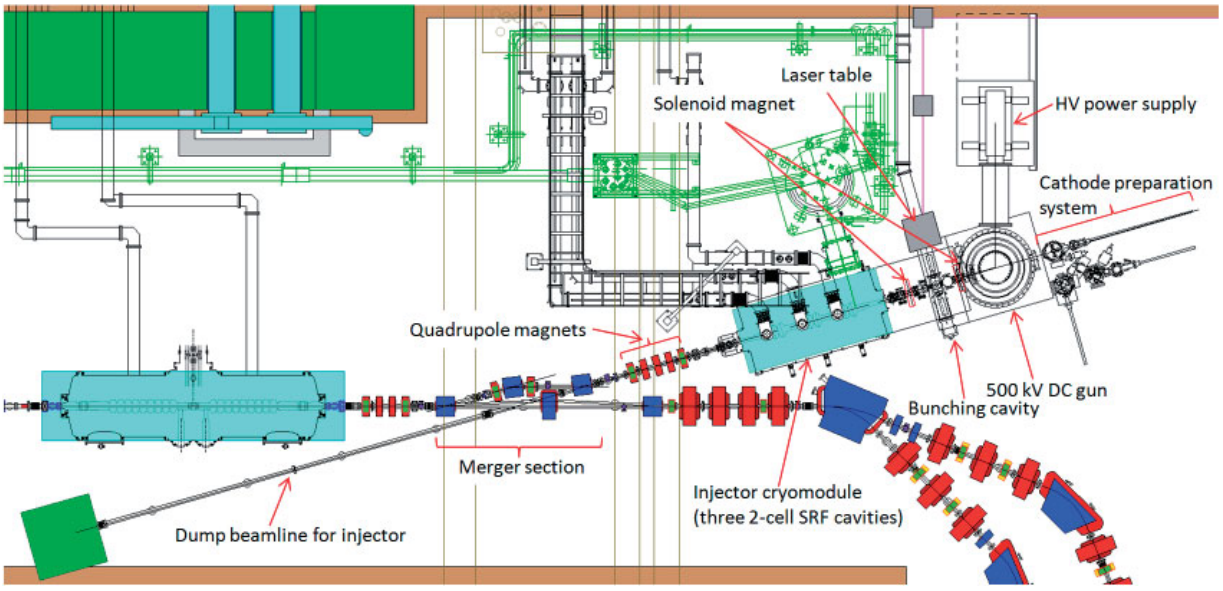

Figure 2
Design layout of cERL injector.

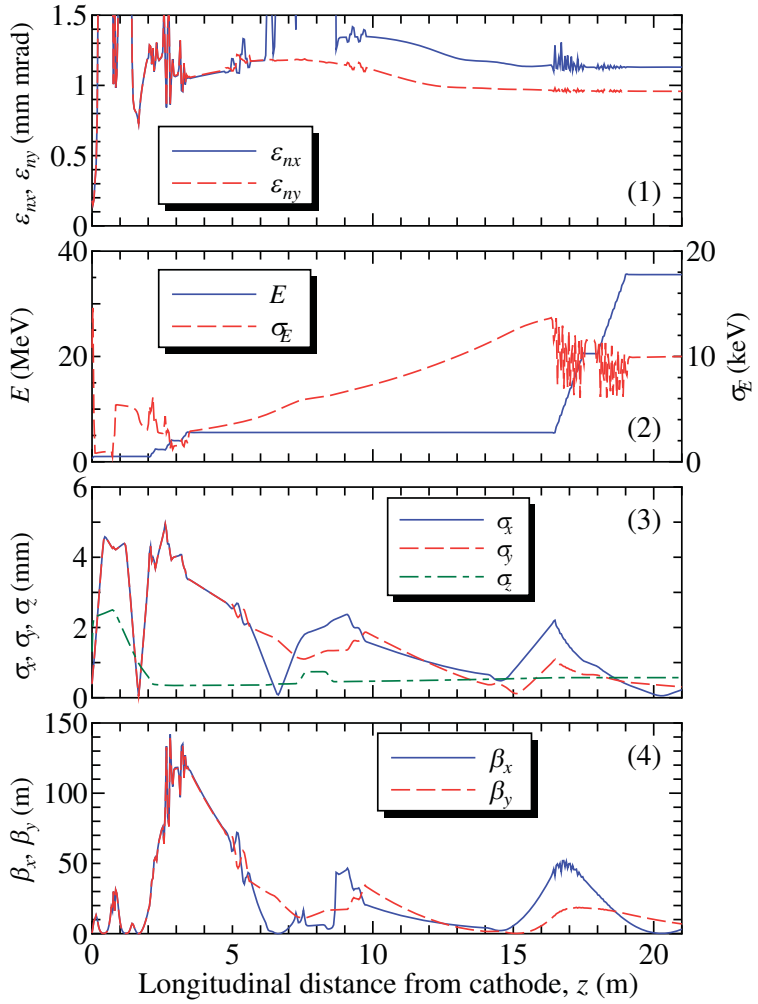

Figure 3
Example of beam envelopes from the gun to the matching point (an exit of the first main-linac cavity) using optimized beamline parameters.

Table 2 Parameters of the injector beamline which correspond to the optics design shown in Fig. 3. Note that further optimization is in progress.

Full width of laser pulse	16 ps
Spot diameter of laser light	0.38 mm
DC gun voltage	500 kV
Magnetic field of 1st solenoid	0.0326 T
Magnetic field of 2nd solenoid	0.0318 T
Voltage of bunching cavity	90.6 kV
E_{acc} of 1st injector SC cavity	6.46 MV/m
E_{acc} of 2nd injector SC cavity	7.52 MV/m
E_{acc} of 3rd injector SC cavity	6.84 MV/m
Offset phase of 1st injector SC cavity	13.6 degrees
Offset phase of 2nd injector SC cavity	4.8 degrees
Offset phase of 3rd injector SC cavity	10.0 degrees

4-2-2 Design of Return Loop

For the initial commissioning of the cERL using a single return loop, we designed the magnet lattice (see Fig. 4) and calculated the beam optics from the injector to the beam dump consistently. First, two isochronous arc sections were designed so that small normalized emittance could be preserved well against the CSR effects. The lattices and optics of the two arc sections were designed to be identical; the beam optics of each arc section were designed to be symmetrical about the center of the arc where both of the horizontal and vertical betatron functions were chosen to be 5 m. Next, we optimized an arrangement of eight quadrupole magnets between the main SC-cavity module and the 1st arc section so that we could match flexibly the beam optics between the injector and the return loop at a beam energy of 5 MeV with a bunch charge of 7.7 pC. Finally, we designed consistent optics from the injector to the beam dump. The latest layout of the 35-MeV cERL lattice is shown in Fig. 4. The betatron and dispersion functions of the return loop (from the quadrupole magnet just after the cavity cryomodule to the beam dump) are shown in Fig. 5. In these optics, the maximum betatron function is lower than 30 m; the maximum horizontal and vertical beam sizes are 3.4 mm and 1.2 mm, respectively, at a bunch charge of 7.7 pC. In future, we will optimize the beam optics individually for different operation conditions such as a bunch charge of 77 pC, the beam energy of 125 MeV, and those under bunch compression mode.

We designed and fabricated a prototype of the sector bending magnet for the return loop. The principal parameters and a photograph of the prototype magnet are shown in Table 3 and Fig. 6, respectively. The bending magnet was made by laminating adhesive silicon steel sheets of 0.5-mm thickness. The rectangular magnetic core was cut to a trapezium shape after baking the laminated steel for thermocompression bonding. Since the beam energy of cERL will be increased from 35 MeV to 245 MeV step by step, the good-field region of the bending magnet should be wide horizontally over a wide range of beam energy. Therefore, silicon steel, which has sufficient permeability at low magnetic field (μ_s>5000 at B ~0.1T), was chosen. Field measurements of the prototype magnet will be performed soon.

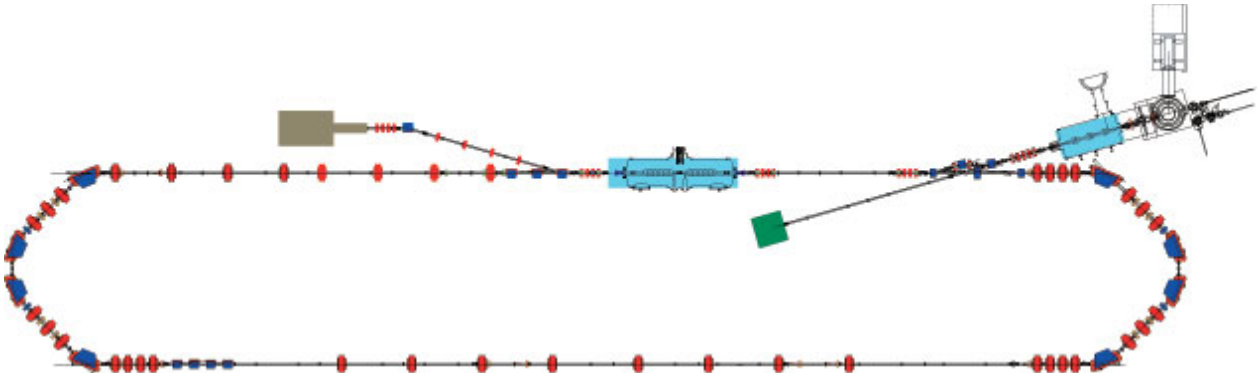

Figure 4
Layout of 35-MeV 1-loop cERL.

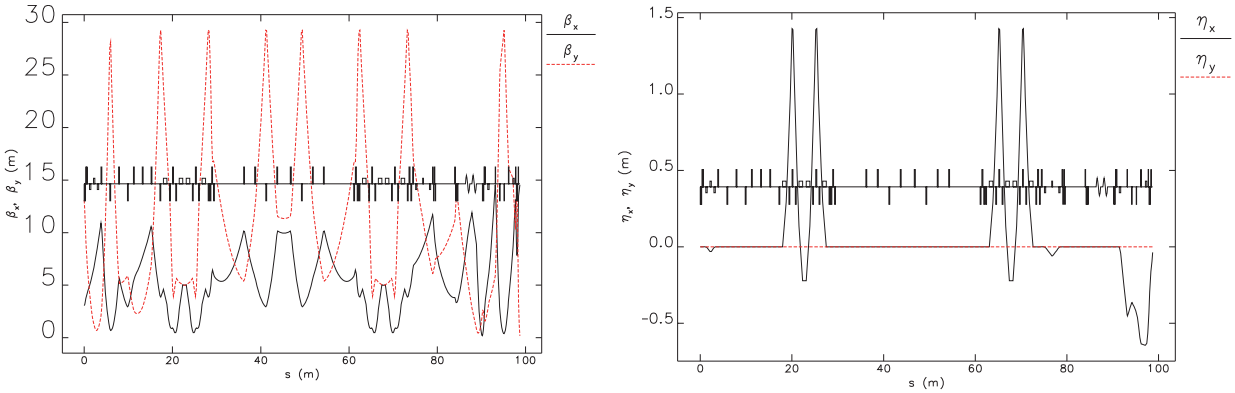

Figure 5
Betatron functions (left) and dispersion function (right) of the cERL return loop.

Figure 6
Bending magnet prototype for cERL.

Table 3 Parameters of the cERL bending magnet prototype.

Parameter	Value	Unit
Maximum core length	820	mm
Curvature radius	1	m
Bending angle	45	degrees
Magnet core shape	Sector (trapezium)	
Cross sectional shape of the core	C-type	
Minimum vertical pole gap	58	mm
Horizontal pole width	230	mm
Number of turns of the coil	56	turns
Material of the core	50H250 silicon steel (Nippon Steel Co.)	
Thickness of each silicon steel sheet	0.5	mm
Design current	752	A
Design voltage	20	V
Maximum beam energy	245	MeV

4-3 Status of Construction

The East Counter Hall at KEK was selected as the construction site for the cERL. This hall was fully renovated in 2009, at which time we removed large amounts (about 10,000 tons) of concrete blocks and radioactive components from the old proton beamlines in the hall in collaboration with the staff of the Institute of Particle and Nuclear Studies (IPNS). In 2010, remaining radioactive matter, such as radioactive iron plates attached to the floor and a lot of polyethylene shielding stuffed in the floor pit, was removed. After this renovation, the East Counter Hall was renamed as the “ERL Test Facility”. Figure 7 shows an inside view of the ERL Test Facility after the renovation. In March 2011, the Great East Japan Earthquake struck, but fortunately the ERL Test Facility and related facilities remained intact.

In parallel with cleaning the hall, we started designing the radiation shielding for the cERL. After checking the maximum safety load of the floor, the structure of the radiation shielding was designed, as shown in Fig. 8. The shielding will be made of reinforced concrete, and the thicknesses of the surrounding wall, inner wall, and ceiling block were chosen to be 1.5 m, 1.8 m and 1.0 m, respectively. The ceiling blocks can be removed when large instruments are installed in the shield. We carried out structural calculations for the structure shown in Fig. 8, assuming both horizontal and vertical loads (acceleration) of 0.5 G, and confirmed that it is strong enough.

The radiation shield will be constructed between the autumn of 2011 and the summer of 2012. Thereafter, the cERL components will be installed until the end of FY2012.

Figure 7
View of the ERL Test Facility after its renovation and clearing.

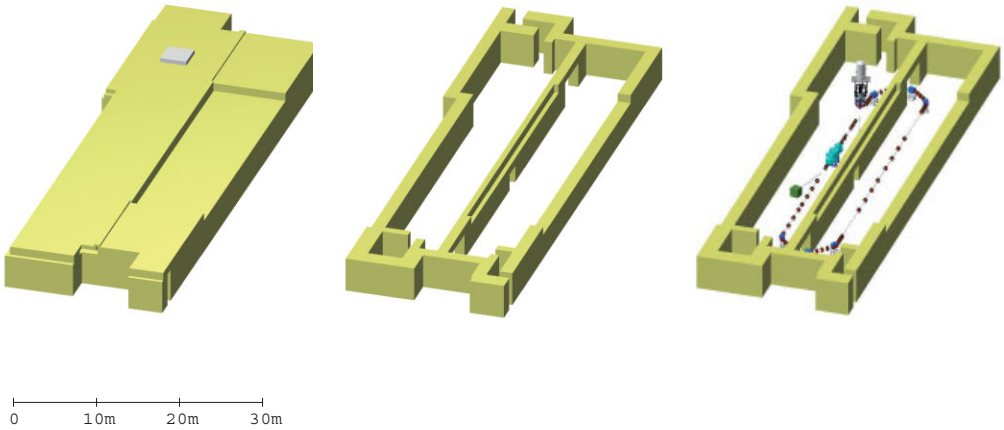

Figure 8
Design of the radiation shield for the cERL.

4-4 High-Brightness Electron Gun

4-4-1 High-Brightness Photocathode DC Gun

The electron sources for the ERLs should produce both low-emittance and high-current (that is, high-brightness) beams. For this purpose, we are developing two photocathode DC guns at the Japanese Atomic Energy Agency (JAEA) and at KEK. These gun-development programs are closely related, and aim to achieve a normalized beam emittance of less than 1 mm·mrad with sufficiently-long cathode lifetime. To suppress emittance growth due to the space-charge effect, the gun voltage should be 500 kV or higher. An extreme-high vacuum (order of 10^{-10} Pa) of the gun chamber is required to preserve a Negative Electron Affinity (NEA) surface of the cathode. Thus, all of the vacuum components in the gun system (titanium chamber, ceramic insulators, guard rings, etc.) should have a very low outgassing rate, and the pumps should function under the extreme-high vacuum.

With the first gun developed at JAEA, we succeeded in extracting electron beams of 5.7 μA at a gun voltage of 300 kV; we could also apply a high gun voltage of up to 500 kV by installing a cathode electrode and NEG pumps [3]. The pressure in the gun chamber reached 6×10^{-10} Pa (N_2 equivalent pressure) using 18000 l/s NEG pumps after baking at 180°C for 50 hours. The 1/e static lifetime of the NEA GaAs cathode is 1000 hours in a cathode preparation chamber (see Fig. 9).

The second gun (Fig. 10), developed at KEK, was constructed from a gun chamber and a pair of ceramic insulators; guard-ring electrodes were fixed in the in-

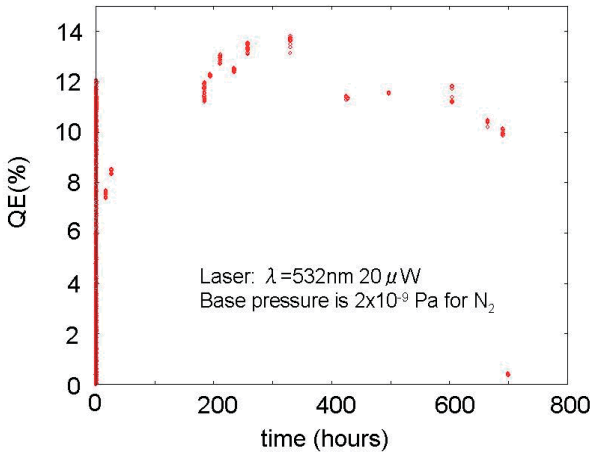

Figure 9
Measured static lifetime of NEA GaAs cathode in the cathode preparation system of the 1st gun system.

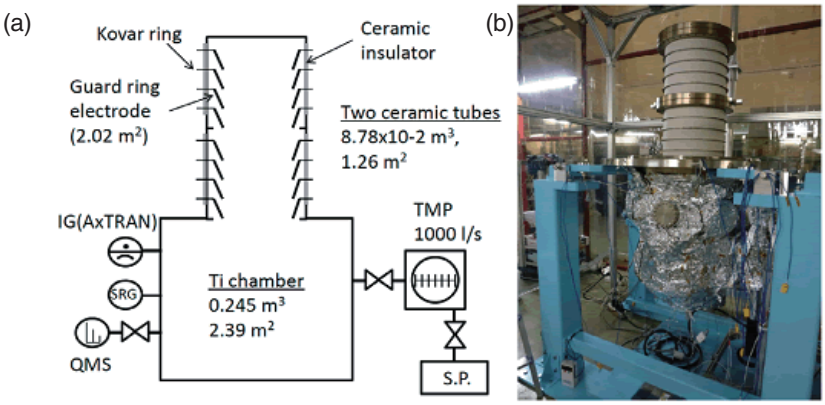

Figure 10
Schematic drawing (a) and photograph (b) of the vacuum system of the 2nd gun at KEK.

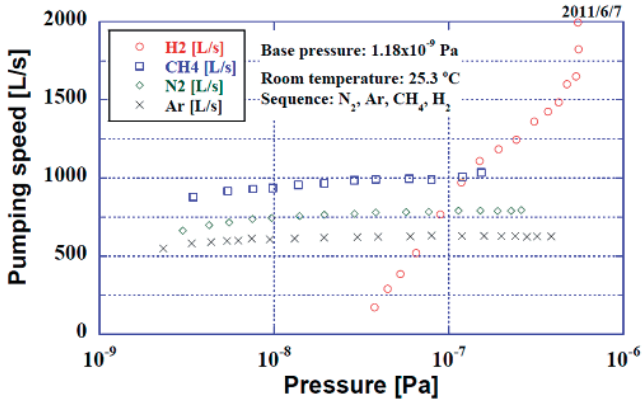

Figure 11
Measured result of pumping speed of 20-K bakeable cryopump under vacuum pressures ranging from 10^{-7} to 10^{-9} Pa.

side of these ceramic insulators. In order to clarify the actual performance of the vacuum system, we precisely measured its outgassing rate by the rate-of-rise (RoR) method [4]. The gun system was baked at temperatures between 150ºC to 200ºC for 100 hours. After the baking process, a total outgassing rate of 1.0×10^{-10} Pa m^3/s (H_2 equivalent) was measured.

The pumping speed of a bakeable cryopump has been measured by using a standard conductance element which was developed by AIST. The preliminary result for the 20-K bakeable cryopump is shown in Fig. 11. High pumping speeds were measured for N_2, Ar, and CH_4 gases in a pressure range of 10^{-9} Pa, however, the pumping speed for H_2 was limited under ultra-high vacuum because cryo-condensation of H_2 was impossible at 20 K. For the actual installation to our electron-gun system, we plan to use a 4-K bakeable cryopump in order to generate extreme-high vacuum of less than 1×10^{-10} Pa.

REFERENCES

[3] N. Nishimori R.Nagai, R.Hajima, M. Yamamoto,T. Miyajima, Y. Honda, H.Iijima, M. Kuriki, M. Kuwahara, S. Okumi, and T. Nakanishi, *Proc. the 8th Annual Meeting of Particle Accelerator Society in Japan*, MOPL05 (to be published) .

[4] M. Yamamoto H. Yoshida, H. Kurisu, T. Honda, Y.Tanimoto, T. Uchiyama, T. Nogami and M. Kobayashi, *Proc. the 8th Annual Meeting of Particle Accelerator Society in Japan*, TUPS160 (to be published).

4-4-2 Drive Laser for the Gun

A drive-laser system for the photocathode gun should produce laser pulses having a repetition rate of 1.3 GHz, pulse duration of 20 ps, and an average power of 15 W. The wavelength was originally specified to be ~800 nm to realize the lowest emittance, however, we have recently found that a wavelength of approximately 500 nm may be a better choice, based on our studies on the emittance and time response of photocathodes. A stable oscillator that can be synchronized to the accelerator timing system, a high power amplifier, and a wavelength conversion system are the main items in the laser system. There are also various issues that are related to beam operation, such as spatial and temporal

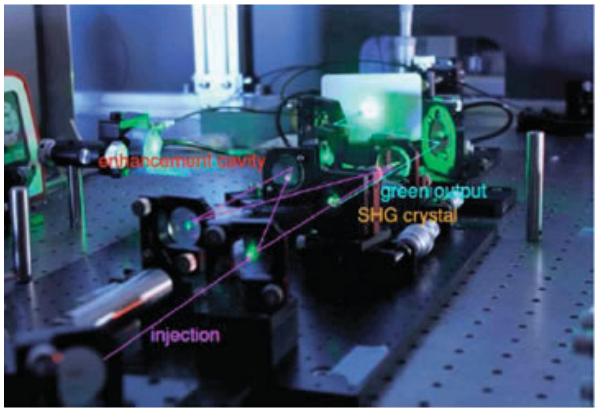

Figure 12
Laser system with cavity wavelength conversion.

shaping, various operational modes of pulse structure, delivery to the gun, position and intensity control, fast interlock system, and so on.

Work on developing the drive laser system has been carried out in AIST and ISSP. Using a fiber amplifier, an average laser power of about 10 W, and recently 30 W, was demonstrated at a wavelength of 1035 nm [5]. Using this laser, generation of second harmonic light was also demonstrated. With an input laser of 10 W (150 nJ/pulse), conversion efficiency of about 50% was obtained at a repetition rate of 85 MHz and a pulse duration of 1 ps. Scaling this result for the peak intensity would achieve 300 mW at a repetition rate of 1.3 GHz. Thus, improving the conversion efficiency is the key issue for a high repetition rate system.

At the gun test stand of KEK, we have introduced a commercially-available 1.3-GHz laser oscillator and a fiber amplifier, and have studied the performance of the oscillator. Although the long-term stability is still questionable, we confirmed that it could operate in a mode-lock state synchronized to the given RF reference. In order to improve the wavelength conversion efficiency, a new scheme utilizing an enhancement cavity (see Fig. 12) has been proposed and tested.

REFERENCE

[5] I. Ito, T. Kawasaki, N. Nakamura, D. Yoshitomi, Y. Kobayashi, K. Torizuka and Y. Honda, *Proc. IPAC'10*, (2010) 2141.

4-4-3 Beam Test and Cathode Development at Gun Test Stand

We started constructing a gun test stand (Fig. 13) in 2009. The purpose of the test stand is to proceed with beam commissioning at the injector system in parallel with constructing the main part of the cERL. At present, the 200-kV electron gun, which was transferred from Nagoya University, is connected to the beamline, but in future the beamline will be switched to the 500-kV gun now being developed.

The test beamline consists of three sections, as shown in Fig. 14. The first section is the injector line which is the low energy region exactly the same as the one to be installed in the cERL. This is a short line but important in order to realize the beams that are required at the cERL. It has two solenoid magnets to compensate emittance growth due to space-charge force, and a buncher cavity to give velocity modulation. Screen monitors, BPMs, and corrector magnets are necessary to create a well-defined initial beam to be accelerated. There is also a laser input chamber, which works as a vacuum pumping system. The second section is the diagnostic line, which has screen monitors and slit scanners. The waist scan method, which measures the evolution of beam size with screen monitors while changing the focusing strength of a solenoid magnet, is routinely used to measure emittance at a low charge. At a higher charge, under which the beam dynamics are dominated by the space-charge effect, the slit scan method will be used. An RF deflector cavity projects the temporal profile of a bunch to a spatial profile on a screen monitor, which can be used to measure the bunch length. The third section is the dump line. At high current operation, the entire beam current should be transferred to the dump, where heat must be removed and gas suppressed to achieve stable beam operation.

After initial commissioning of various hardware, we started beam studies in the autumn of 2010. Procedures to tune the beam orbit through the diagnostic line have been established, using a beam-based technique to sense the magnetic center of solenoid magnets. Various beam optics settings suitable for each measurement such as emittance, bunch length, charge distribution on the cathode, etc. were checked and routinely reproduced so that we could carry out reliable measurements.

The first study items were to measure the beam properties at a low charge where space-charge effects could be ignored. With the well-tuned diagnostic beamline, this gives us information about the initial distribution of electrons at the cathode surface.

The first measurement was carried out with a commercially-available bulk GaAs cathode. The emittance measurement was carried out under different conditions of illuminating-laser wavelengths, namely 544 nm and 785 nm. In the design report on the cERL [6], it was expected that a much lower emittance would be obtained with a laser wavelength of approximately 800 nm than with 500 nm because of the smaller residual electron energy with respect to the bandgap. Although the beam had a slightly higher emittance at the shorter wavelength, the results clearly showed that the emitted electrons were greatly relaxed compared with the excitation energy. This result indicates that the wavelength of approximately 500 nm would be good enough to realize the required emittance. This is good news for the overall design of the electron gun system because it can simplify the laser system and has advantages in terms of quantum efficiency and life time of the cathode.

The temporal response of cathodes has been measured using the deflector cavity system. When the

Figure 13
Picture of gun test stand.

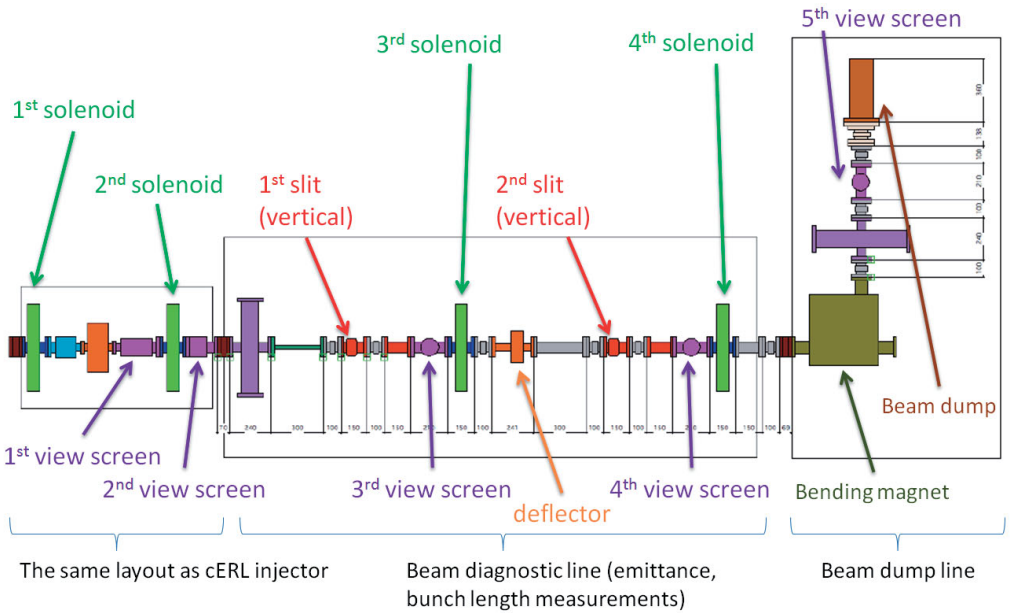

Figure 14
Layout of test beamline.

wavelengths of the laser were chosen to be close to the bandgap energy, a long tail was observed. This is a known phenomenon resulting from a long photo-absorption length and a finite diffusion speed of electrons in the cathode.

In order to investigate this quantitatively, we made special cathodes that had thin defined thicknesses in collaboration with Nagoya University. It was confirmed that the response time was improved with thinner cathodes, and could be understood with a diffusion model of electron dynamics in the cathode. A typical result of the temporal response of photocathodes having different thickness of active layer is shown in Fig. 15. The active layers for the samples with the thicknesses of 300 nm and 1000 nm were grown on $Al_{0.4}Ga_{0.6}As$ buffer layer. The measured photoemission response depends on the active layer thickness and doping density at a laser wavelength of 785 nm.

One of the most challenging issues in the ERL gun is the operational lifetime of the cathode under high beam currents. After continuous operation for more than 10 hours, noticeable degradation in the quantum efficiency was seen even at the beam current of only 0.1 mA. Mapping the quantum efficiency distribution on the cathode, it was found that there was local damage, which indicates ion back-bombardment. Studies to solve this problem are necessary for reliable operation at the cERL.

REFERENCE

[6] R. Hajima, N. Nakamura, S. Sakanaka and Y. Kobayashi (ed.), *KEK Report* 2007-7 (2008)/*JAEA-Research* (2008) 032.

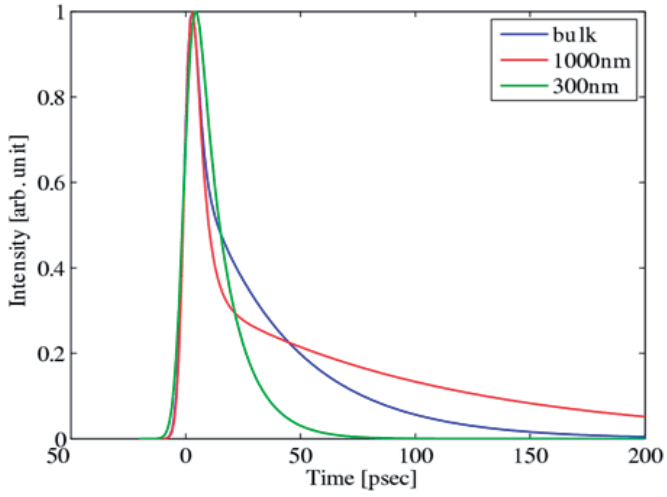

Figure 15
Measured result of temporal response of NEA GaAs photocathode by irradiating short laser pulses (~ ps, λ = 785 nm) to samples having thicknesses of 300 nm, 1000 nm, and a bulk sample. The Zn doping concentration was controlled to be 1.5×10^{18} cm^{-3} for the 300 nm and 1000 nm samples, and to be 1.4×10^{19} cm^{-3} for the bulk sample.

4-5 Superconducting Cavities

4-5-1 Two-Cell Cavity for the Injector [7-11]

An injector for the ERL light source is required to accelerate CW electron beams (maximum beam current: 100 mA) from the beam energy of 0.5 MeV to 10 MeV (or 5 MeV in the cERL). In this application, the critical hardware components are not the cavities but the RF input couplers and higher-order-mode (HOM) dampers. An injector cryomodule containing three 2-cell cavities was designed for the cERL (10 mA, 5 MeV), as shown in Fig. 16. The cavities are dressed with a He vessel made of titanium, and magnetic shields are put inside the He vessel. The estimated cryogenic loads in 100 mA and 10 MeV operation are a total of 26 W at 2 K and 55 W at 4.5 K as the sum of the static and dynamic heat loads. It is critical to remove the dynamic heat load of the input couplers (4 W at 2 K, 16 W at 4.5 K) and HOM power extraction cables (7 W at 2 K, 4 W at 4.5 K). They are anchored to 4.5 K He-reservoir panels placed on both sides of the cavities, which work as a thermal shield as well.

A three 2-cell cavity system was chosen for the cERL injector. Each cavity is driven by two input couplers to reduce the required power handling capacity and also to compensate the coupler kick. A HOM coupler scheme was chosen for HOM damping, and five HOM couplers are attached on both beam pipes of each cavity. The completed three 2-cell cavities to be installed in the injector cryomodule are shown in Fig. 17. They have a TESLA-like cell shape and a larger beam pipe aperture of 88 mm. A vertical test of the first 2-cell cavity was carried out recently, using the set-up shown in Fig. 18. As a result of the improved cooling at feed-throughs of the HOM pick-up probes, an accelerating gradient of 25 MV/m, which exceeded the specifications, was successfully maintained under a CW operation in the vertical tests. Vertical tests of the other two 2-cell cavities will be successively carried out in the autumn of 2011. Newly-developed feed-throughs with more efficient cooling will also be tested in these vertical tests.

The RF input coupler is the most critical component in a high-power application of superconducting (SC) cavities. A coaxial coupler with a single disk-type ceramic window developed for TRISTAN SC cavities is used for input couplers for the injector. The completed six input couplers to be installed in the injector cryomod-

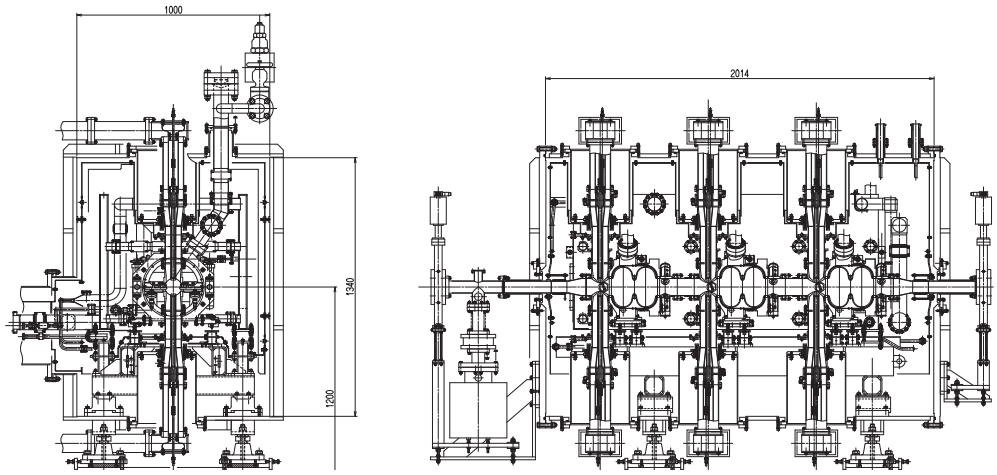

Figure 16
Design of the cERL injector cryomodule.

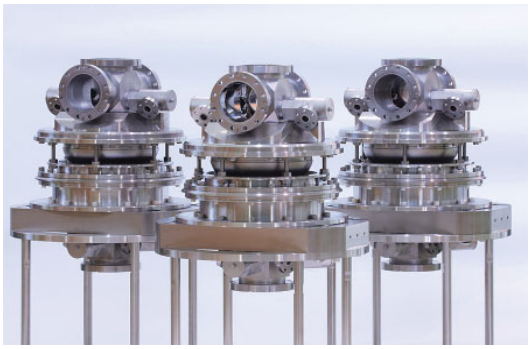

Figure 17
Three 2-cell cavities for the injector cryomodule.

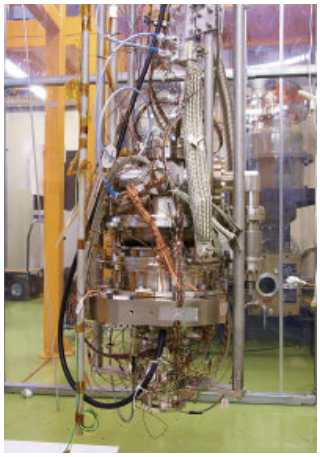

Figure 18
Set-up of vertical test of the first 2-cell cavity for the injector cryomodule.

Figure19
Six input couplers for the injector cryomodule.

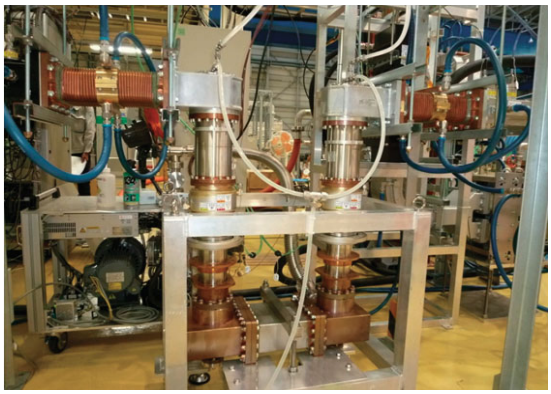

Figure 20
High power test stand for RF conditioning of two prototype input couplers.

ule are shown in Fig. 19. The impedance of the coaxial part was changed from 41 Ω of the prototype couplers to 69 Ω in order to reduce RF losses on a Cu surface, and the outer diameter is 82 mm. The input couplers are assembled with cavities in a clean room before installation in the cryomodule, so they should be as short as possible. Then, thermal interception becomes difficult, requiring 5 K and 80 K anchors at the outer conductors. The inner conductors and the RF windows are cooled by water. High power tests of a pair of the prototype input couplers, as shown in Fig. 20, were performed by using a newly-developed 300-kW CW klystron. The input couplers were successfully processed up to 100 kW in a pulsed operation with a duty of 10% and 50 kW in a CW operation for 30 minutes.

Assembly of the cERL injector cryomodule will be started in February 2012, and the first cool-down test of the cryomodule is scheduled in May 2012.

REFERENCES

[7] K. Watanabe, H. Hayano, S. Noguchi, E.Kako and T. Shishido, *Proc. SRF'2007* (2007) 530.
[8] K. Watanabe S. Noguchi, E. Kako, T. Shishido, Y. Yamamoto, K. Umemori and M. Sato, *Proc. SRF'2009* (2009) 359.
[9] E. Kako, S. Noguchi, M. Sato, T. Shishido, K. Watanabe, Y. Yamamoto, H. Jenhani and T.X. Zhao, *Proc. SRF'2009* (2009) 485.
[10] S. Noguchi, E. Kako, M. Satoh, T. Shishido, K. Watanabe and Y. Yamamoto, *Proc. IPAC'10* (2010) 2944.
[11] K. Watanabe, E. Kako, S. Noguchi, M. Satoh, T. Shishido and Y. Yamamoto, *Proc. LINAC10* (2010) 401.

4-5-2 Nine-Cell Cavity for the Main Linac

There has been appreciable progress toward the construction of the cERL main-linac cryomodule. Several prototypes of components, such as cavities, input coupler and HOM absorbers, were fabricated and their performance has been investigated. The results of investigations and the plan for cryomodule construction are described below.

Nine-Cell Cavity

The most important issue for the main-linac cavity is strong damping of HOMs for avoiding beam-breakup (BBU) instability, which is critical for recirculating a high beam current of more than 100 mA. On the other hand, a moderate accelerating field of 15 – 20 MV/m is required. To obtain efficient damping of HOMs, the KEK-ERL model-2 cavity [12] is designed with a large iris diameter of 80 mm. As a side effect, this design results in increased electric fields on the cavity surface, so it is essential to overcome field emission for CW operation.

Two prototype cavities, cavity #1 and #2, were fabricated. Cavity #1 is a prototype to investigate the designed cell shape and the eccentric fluted beampipe structure. Cavity #2 is a prototype of the model to be installed in a cryomodule, while satisfying the requirement of the High Pressure Gas Safety Act. As shown in Fig. 21, He jacket end plates and stiffener rings are manufactured. The niobium thickness is increased for both halves of the end cells. Helicoflex is used for vacuum sealing.

Cavity performance was investigated by vertical tests for cavities #1 and #2. Figure 22 shows vertical test results for cavity #1 [13, 14]. From the 1st to 8th measurement, the cavity suffered from field emissions. After optimizing the parameters for electro-polishing (EP), as well as careful cavity assembly, maintaining the clean condition, and so on, the cavity finally reached 25 MV/m under the condition of small field emissions. These results satisfy the specification for the ERL main linac.

Figure 23 shows vertical test results for cavity #2. For all measurements, the field exceeded 20 MV/m. For all cases, field limitations are quenches due to field emissions. Note that the Q values are somewhat low in the plots of Fig. 23. In these plots, the Q-E curves are for the final state, i.e. taken at the end of the vertical test. There are two reasons: the use of stainless-steel flanges for the measurements, and the degradation of Q values during processing. It was observed that Q values gradually decreased during processing in π-mode or pass-band modes, for both the first and second vertical tests.

After the second vertical test, the cavity was only warmed up, without additional treatment, and the third vertical test was carried out in order to investigate the possible cause of this Q degradation. If it is caused by damage on the niobium surface, it is expected that the

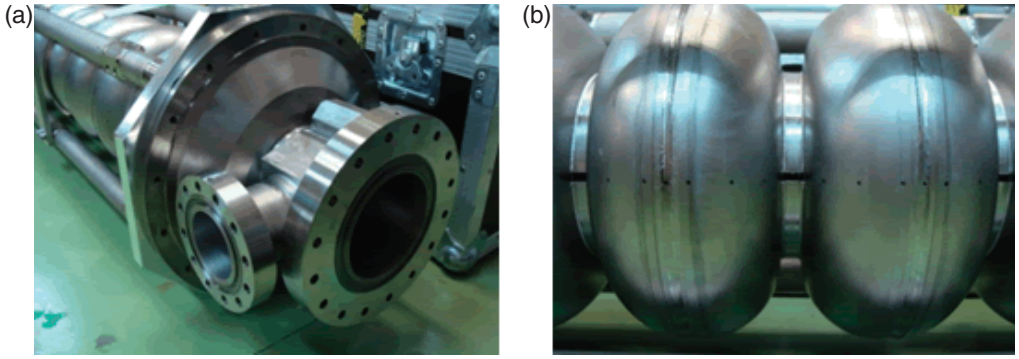

Figure 21
Prototype 9-cell cavity #2. (a) titanium end plate for He jacket and flanges, and (b) stiffener rings.

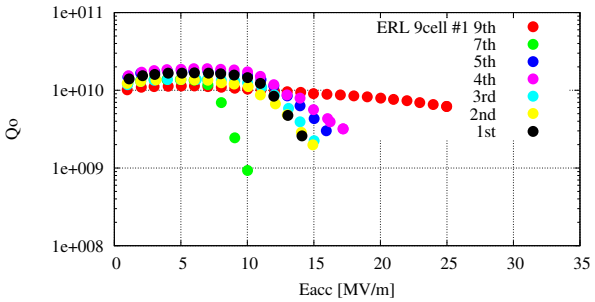

Figure 22
Vertical test results for prototype main-linac 9-cell cavity #1.

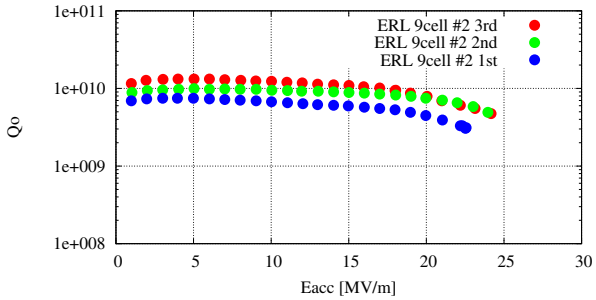

Figure 23
Vertical test results for prototype main-linac 9-cell cavity #2.

Q values would not recover after warming-up. The results are shown by red dots in Fig. 23. The Q values at the lower field recovered to the initial value in the second vertical test. The cause of Q degradation is considered to be trapping of magnetic field during processing. On the other hand, the Q values at higher field were the same as the final value of the second vertical test. This is because field emitters do not change the situation after warming-up. Details of the vertical test results for cavity #2 are described in [15].

Input Coupler

Because of the energy recovery, no beam loading effect is considered for main-linac cavities. The requirement for the input coupler is that the cavity field should be kept stable, under the detuning effect due to microphonics. Assuming a maximum detuning of 50 Hz and external Q to be 2×10^7, maximum RF power of 20 kW is required to keep the cavity field stable. The input coupler has two windows, a warm and a cold window, to prevent dust contamination of the cavities. A variable coupling mechanism is realized by using bellows. The inside of an inner conductor is cooled by nitrogen gas. The details of the coupler design are given elsewhere [16].

As shown in Fig. 24 (a), a prototype input coupler was fabricated in order to check its performance. A high-power test stand was constructed in the ERL Test Facility at KEK. The experimental setup is shown in Fig. 24 (b). In order to simulate the conditions inside the cryomodule, the input coupler was installed in a vacuum chamber and the cold window was cooled by liquid ni-

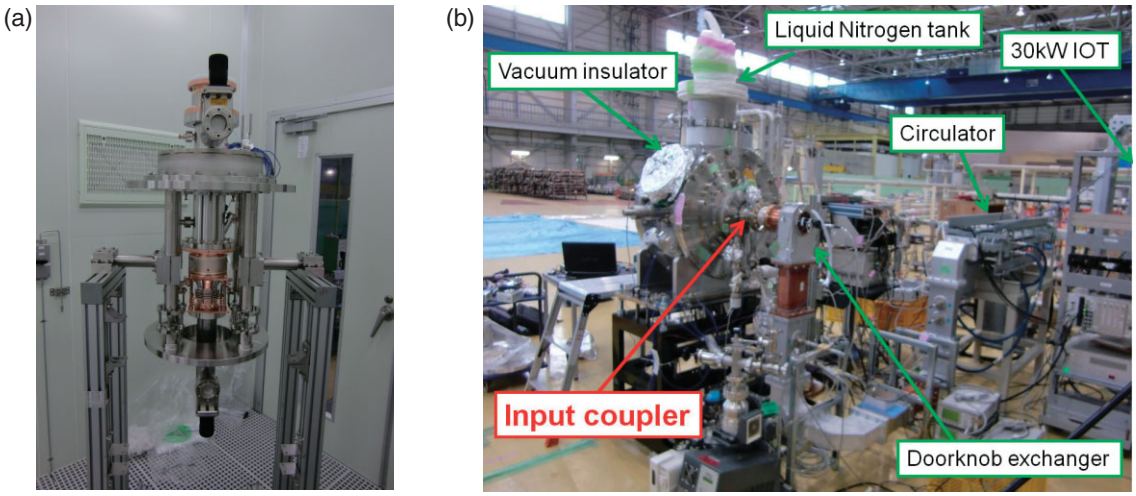

Figure 24
(a) prototype of input coupler. (b) setup for high power test for input coupler, at 80 K.

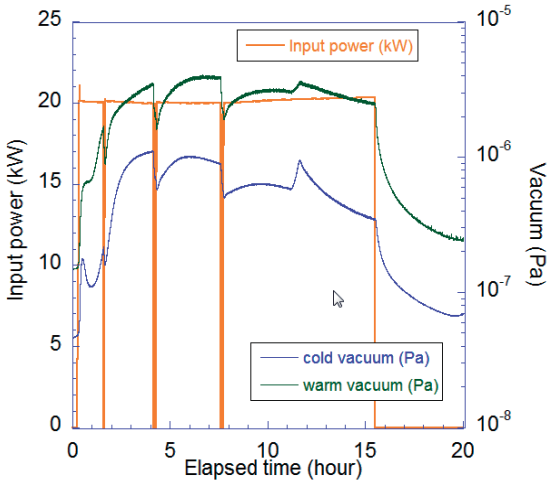

Figure 25
High power test stand for RF conditioning of two prototype input couplers.

trogen. RF power was produced by a 30 kW inductive output tube (IOT), passed through the coupler, and then reflected by an end plate. Thus, the coupler was processed under a standing wave.

In the initial trial of the high power test, RF power was smoothly increased and reached 20 kW. At a power of 20 kW, however, there was a sudden discharge accompanied by an arc and vacuum interlocks. Thereafter, the input power was limited to 10 kW and the normal processing procedure did not help to increase the input power. A pulse processing method was applied and the situation gradually improved. After the pulse processing for eight hours, RF power reached 25 kW, and then was kept at 20 kW. Figure 25 shows that RF power was successfully kept for 16 hours. During this test, the input coupler was sufficiently stable, except that the arc sensor was triggered three times by noise. The measured temperature rise was adequate. Details of the high power test are described in [17].

After the high power test with cooling, a thermal cycle test was conducted. After ten thermal cycles between room temperature to 80 K, no leaks were observed and no cracks were found in the ceramic windows. Thus, the high power test and thermal cycle tests showed that the input coupler satisfies the specifications of the ERL main linac.

Beampipe HOM Absorber

To damp HOMs efficiently, beampipe HOM absorbers are used. The HOM absorber will be installed in a cryomodule and kept at 80 K. After investigating the RF characteristics at low temperature, one ferrite, IB004, was selected as a material for HOM absorption.

Two kinds of prototype were fabricated. One type is shown in the upper part of Fig. 26, and is called the HOM absorber model with hot-isostatic pressing (HIP) ferrite. HIPped ferrite is attached on the inner surface of the copper base. HOM absorption measurements and thermal cycle tests are now being conducted using this model [18]. Another type is shown in the lower part of Fig. 26, and is called the HOM absorber model without HIP ferrite. It has almost the final structure, including the comb-type RF bridge on the inside and bellows on the outside of the HOM absorber, but no ferrite was attached. The thermal properties of the HOM absorber were studied using this HOM absorber model without HIP ferrite [18,19]. The HOM absorber model was installed in the adiabatic vacuum chamber, which is the same as that used for the input coupler tests, and cooled down to liquid nitrogen temperature. The thermal resistance of the bellows was measured and found to be no problem. Cooling ability against HOM absorption power was also checked by supplying power to heaters, which were attached on the inner surface of the model.

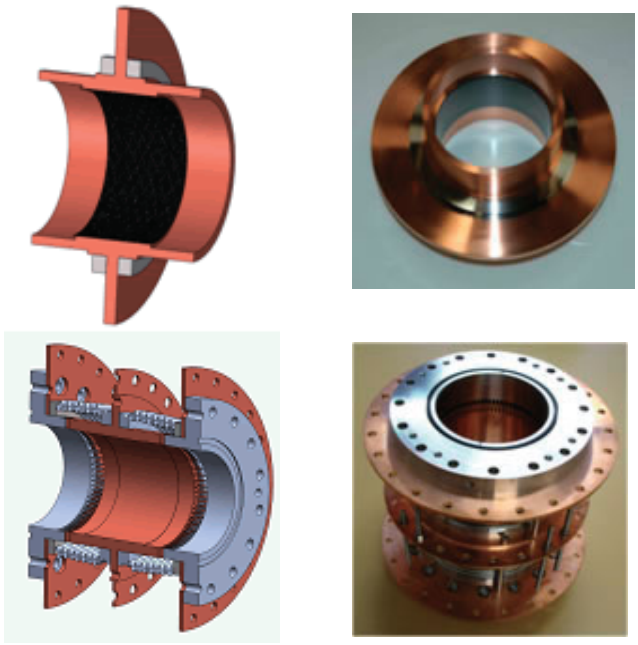

Figure 26
Schematic views and photographs of HOM absorber models with HIP ferrite (upper) and without HIP ferrite (lower).

The obtained temperature distribution was used for detailed design of the main-linac cryomodule.

Cryomodule

For the initial stage of the cERL, one cryomodule with two 9-cell cavities will be constructed. Its design is shown in Fig. 27. Slide-Jack and piezo tuners are used for frequency tuning. Two 9-cell cavities, cavity #3 and #4, were fabricated. After surface treatment, vertical tests will be performed in the autumn of 2011. Two input couplers, three HOM absorbers and two Slide-Jack tuners are being fabricated. Coupler aging will be carried out in winter. He jackets will be mounted on the cavities, and a cryomodule will be assembled around 2012.

REFERENCES

[12] K. Umemori, T. Furuya, S. Sakanaka, T. Suwada, T. Takahashi, H. Sakai, K. Shinoe and M. Sawamura, *Proc. APAC'07* (2007) 570.
[13] K. Umemori, H. Sakai, T. Furuya, S. Sakanaka, T. Takahashi, M. Sawamura and K. Shinoe, *Proc. IPAC'10* (2010) 2950.
[14] K. Umemori, T. Furuya, H. Sakai, T. Takahashi, M. Sawamura and K. Shinoe, *Proc. LINAC'10* (2010) 404.
[15] E. Cenni et al., *Proc. SRF2011* (to be published).
[16] H. Sakai,T. Furuya, S. Sakanaka, T. Takahashi, K. Umemori, A. Ishii, N. Nakamura, K. Shinoe and M. Sawamura, *Proc. SRF'2009* (2009) 684.
[17] H. Sakai *et al.*, *Proc. SRF2011* (to be published).
[18] M. Sawamura *et al.*, *Proc. SRF2011* (to be published).
[19] M. Sawamura, T. Furuya, H. Sakai, K. Umemori and K. Shinoe, *Proc. IPAC'10* (2010) 2344.

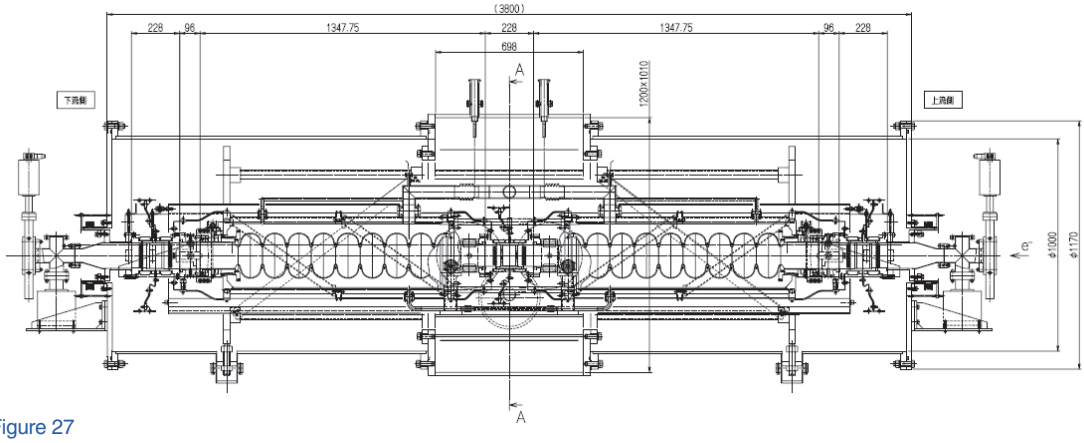

Figure 27
Design of the cERL main-linac cryomodule.

4-6 Cryogenic System

A 2-K helium cryogenic system for the cERL was proposed and designed in FY2008, and its construction was completed in FY2009. The system consists of four major units: 1) a helium liquefier/refrigerator, 2) a set of high-performance helium transfer lines, 3) two 2-K helium refrigerator cold boxes and a helium gas pumping system, and 4) cryomodules of superconducting RF cavities for the injector and the main linac of the cERL. The helium liquefier/refrigerator is equipped with a helium circulation compressor, a helium gas purifier, a 3000-L liquefied helium storage vessel, a helium recovery compressor and gasbags, some of which can be seen in Fig. 28. The high-performance helium transfer lines connect the helium liquefier/refrigerator and two 2-K helium refrigerator cold boxes for the cryomodules as shown in Fig. 29. These cold boxes will be connected

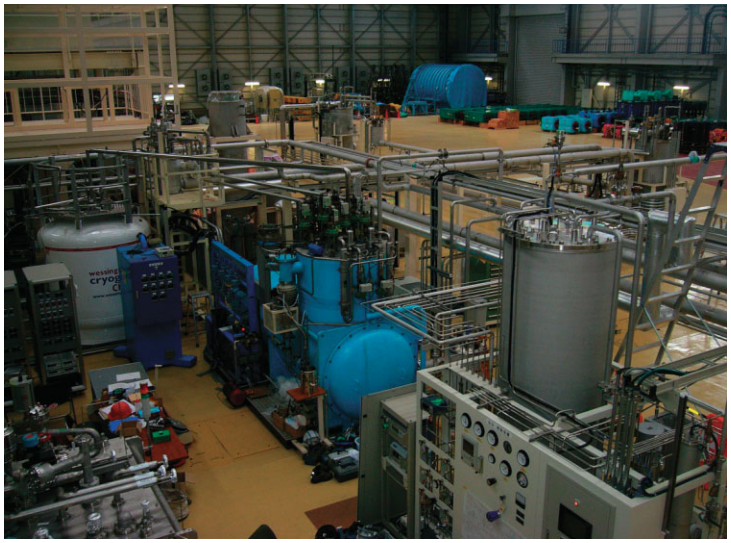

Figure 28
2-K helium cryogenic system for cERL; the light-blue unit (center) is the cold box of the TCF200 helium liquefier/refrigerator, the white vessel (left) is the 3000-L liquefied helium storage vessel, and the white unit with silver cylinder (right) is the helium purifier.

Figure 29
2-K helium cryogenic system for cERL; Two 2-K helium refrigerator cold boxes are ready to be connected to cryomodules of superconducting RF cavities for the injector and main linacs.

to the injector and main cryomodules, respectively, to distribute 2-K superfluid helium, liquid helium for the 5 K thermal shield and liquid nitrogen for the 80 K thermal shield to the cryomodules. In order to operate cryogenic systems, under the High Pressure Gas Safety Act it is necessary to pass completion inspections by the local prefecture (Ibaraki prefecture for KEK). The cryogenic system for the cERL underwent and passed the completion inspection by Ibaraki prefecture in August 2010. By receiving a certification from the prefecture, KEK is officially authorized to operate the cryogenic system.

Since the TCF200 helium liquefier/refrigerator had been originally operated at the National Institute for Materials Science (NIMS) for more than 10 years, the inner surfaces of tubing within it may be contaminated with oil from the helium circulation compressors. This could choke the tubing of the liquefiers/refrigerators and degrade the heat exchange rate of the heat exchangers. We therefore checked the turbo-expanders for any oil adhered over the turbines. Figure 30 is a photo of a rotor of the first-stage turbo-expander. Some oil is clearly visible on a Teflon disk of the rotor. Figure 31 is a photo of the same turbine as that shown in Fig. 30, but taken with black light (ultraviolet light) to clarify the presence of oil on the disk. Less oil was observed in the second-stage turbo-expander, which is located downstream of the first-stage one. Therefore, it is reasonable to conclude that the oil came from the helium compressor, and the amount of oil gradually decreased as it flowed with compressed helium gas through the tubing of the helium liquefier/refrigerator. From these findings, it is concluded that the tubing of the helium liquefier/refrigerator is likely to be contaminated with oil from the compressor. Since it is not allowed to modify the cryogenic system without permission after the completion inspection by the local government, we had to clean up the tubing in situ. We repeatedly introduced liquid solvent into the tubing and discharged it after some duration. Because of the complicated configuration of the tubing in the helium liquefier/refrigerator, it was very hard to drain the solvent

Figure 30
Oil from a helium compressor on a Teflon disk of the first-stage turbo-expander.

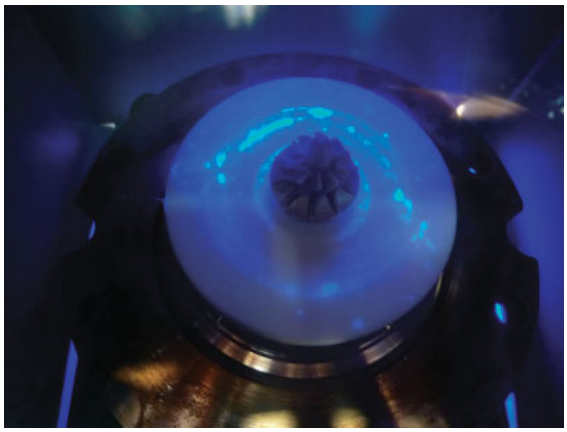

Figure 31
Oil (fluorescent parts with black light) from a helium compressor on a Teflon disk of the first-stage turbo-expander.

Figure 32
Hand-made distiller unit (two storage vessels and one heat exchanger on a red post) for purifying oil solvent from tubing inside the helium liquefier/refrigerator.

completely from the tubing. To avoid environmental contamination, we reused the solvent after purifying it with a hand-made distiller unit (see Fig. 32) to remove oil from the solvent. The hand-made distiller unit consists of two solvent storage vessels and a heat exchanger. One vessel covered with insulation is for the used solvent. This vessel contains an electric heater to warm up the used solvent. The solvent easily evaporates while the oil remains liquid in the vessel. Evaporated solvent is cooled down by cooling water in a heat exchanger, and re-condenses. Then, purified solvent is stored in the second vessel for reuse. We measured the amount of oil removed by the solvent in the storage vessel, and estimated the amount of oil remaining inside the tubing. The amount of oil removed from the tubing gradually decreased as expected, but it seemed to require many more cleaning cycles to remove oil from the tubing completely, so we decided to stop the cleaning when the amount of removed oil no longer varied much.

In January 2011, we operated the helium liquefier/refrigerator for the first time after its installation in the ERL Test Facility. The helium liquefier/refrigerator worked normally, and liquefied helium without any technical problems. The liquefaction rate appeared to be more than 250 L/h, which is the specification value of the helium liquefier/refrigerator. Liquid helium produced by the helium liquefier/refrigerator is transferred and stored in the 3000-L liquefied helium vessel as shown in Fig. 28. Since the success of our first liquefaction with the helium liquefier/refrigerator at the ERL Test Facility, we have operated the helium liquefier/refrigerator several times to store more liquid helium in the 3000-L storage vessel.

On March 11, 2011, the Tohoku-Pacific Ocean Earthquake (now widely called the Great East Japan Earthquake) occurred. Since the helium liquefier/refrigerator was not in operation at that moment, our cryogenic system did not suffer from the earthquake. However, since the electricity supply was cut and limited inside KEK for almost one month after the earthquake, the helium recovery compressor could not be activated during that period, and a considerable amount of evaporated helium gas from the 3000-L storage vessel was released to the atmosphere to avoid excess pressure inside the cryogenic system.

Before connecting our cryogenic system to the cryomodules of the superconducting cavities, we will check the overall performance of the cryogenic system in FY2011. First, we will supply liquid helium to the two 2-K helium refrigerator cold boxes through the high-performance transfer line to check the thermal performance of the cryogenic system. Then, the cooling power at 2 K of the cryogenic system will be measured by activating the helium gas pumping system.